

Circular polarization survey of intermediate polars I. Northern targets in the range $17^{\text{h}} < \text{R.A.} < 23^{\text{h}}$ [★]

O.W. Butters^{1,2}, S. Katajainen³, A.J. Norton¹, H.J. Lehto³, and V. Piirola³

¹ Department of Physics and Astronomy, The Open University, Walton Hall, Milton Keynes MK7 6AA, UK

² Department of Physics and Astronomy, University of Leicester, Leicester, LE1 7RH, UK

e-mail: oliver.butters@star.le.ac.uk

³ Tuorla Observatory, Department of Physics and Astronomy, University of Turku, Väisäläntie 20, FI-21500 Piikkiö, Finland

e-mail: sekataja@utu.fi

Accepted 2007 ???; Received 2007 ???; in original form 2007 ???

ABSTRACT

Context. The origin, evolution, and ultimate fate of magnetic cataclysmic variables are poorly understood. It is largely the nature of the magnetic fields in these systems that leads to this poor understanding. Fundamental properties, such as the field strength and the axis alignment, are unknown in a majority of these systems.

Aims. We undertake to put all the previous circular polarization measurements into context and systematically survey intermediate polars for signs of circular polarization, hence to get an indication of their true magnetic field strengths and try to understand the evolution of magnetic cataclysmic variables.

Methods. We used the TurPol instrument at the Nordic Optical Telescope to obtain simultaneous UBVRi photo-polarimetric observations of a set of intermediate polars, during the epoch 2006 July 31 - August 2.

Results. Of this set of eight systems two (1RXS J213344.1+510725 and 1RXS J173021.5–055933) were found to show significant levels of circular polarization, varying with spin phase. Five others (V2306 Cyg, AO Psc, DQ Her, FO Aqr, and V1223 Sgr) show some evidence for circular polarization and variation of this with spin phase, whilst AE Aqr shows little evidence for polarized emission. We also report the first simultaneous UBVRi photometry of the newly identified intermediate polar 1RXS J173021.5–055933.

Conclusions. Circular polarization may be ubiquitous in intermediate polars, albeit at a low level of one or two percent or less. It is stronger at longer wavelengths in the visible spectrum. Our results lend further support to the possible link between the presence of soft X-ray components and the detectability of circular polarization in intermediate polars.

Key words. stars: binaries – stars: magnetic fields – polarization – infrared: stars

1. Introduction to magnetic cataclysmic variables

Cataclysmic variables (CVs) are a class of binary system in which a main sequence star (the secondary) transfers matter to its white dwarf (WD) companion (the primary), via Roche lobe overflow. Within this class there is a division of systems based upon the magnetic field strength of the WD, the non-magnetic (or only very slightly magnetic) CVs and the magnetic systems (mCVs). This is an important distinction, as the presence of a magnetic field on the WD has a profound effect on the structure and evolution of the system, since the accreting material is a plasma, its motion is subject to the field. In mCVs the accreting material typically attaches itself to the magnetic field lines close to the magnetospheric radius and is funnelled toward the WD surface. If the WD has a dipole magnetic field structure then this has the effect of concentrating the accreting material into small regions above the magnetic poles. The material reaches supersonic speeds as it is accelerated toward the surface under the influence of gravity. It then goes through a shock as it decelerates to subsonic speeds. This matter then cools as it falls to the surface, emitting hard X-rays ($kT \sim 10 - 60\text{keV}$) via bremsstrahlung radiation and optical/infrared cyclotron radiation. Many mCVs also exhibit a soft X-ray component, which

is thought to occur due to either some of the accreting material somehow avoiding the shock and directly impacting the surface of the WD (see e.g. Motch et al. (1996)), or from the reprocessing of hard X-rays (see e.g. Lamb & Masters (1979)). Recently Evans & Hellier (2007) have suggested that this component is in fact present in all mCVs, and that its detection depends on whether geometric factors allow it to be seen or not.

The mCVs are themselves divided into two groups based upon their periodicities, which are in turn assumed to imply different magnetic field strengths. The polars contain synchronously rotating WDs, whilst in intermediate polars (IPs) the WDs rotate asynchronously with respect to the binary orbit.

The polars typically have a magnetic field strength of the order 10–100 MG. This has the effect of channelling the accreting material onto the WD surface before an accretion disc can form. Furthermore, the magnetic field of the WD extends to the body of the secondary and will act to synchronize the spin and orbital periods of the system. Typically the polars are found to have an orbital and spin period of less than two hours. For an overview of polars see e.g. Cropper (1990).

IPs are asynchronous systems, generally *believed* to have a magnetic field strength of approximately 1–10 MG. This smaller field means that matter falls inward toward the WD in much the same way as in non-magnetic CVs. However, at some critical distance from the WD, the magnetic field will begin to dominate, and the accretion process is altered. It then carries on in much the

[★] Based on observations obtained at the Nordic Optical Telescope at the Roque de los Muchachos Observatory in La Palma.

same way as in the polars. For a comprehensive review of IPs see e.g. Warner (1995) or Patterson (1994).

Non-magnetic CVs evolve from long orbital periods (a few hours) to short orbital periods (just over an hour). The proposed explanation for this evolution is magnetic braking and gravitational radiation (King 1988). Both these processes should also be present in mCVs and since IPs generally have a longer orbital period than the polars it was suggested that IPs evolve into polars (Chanmugam & Ray 1984). This hypothesis has not been widely accepted as there is little evidence of strong magnetic fields in IPs. There are however some IPs with a similar magnetic field strength to the polars, up to 30 MG in the case of V405 Aur (Pirola et al. 2008).

Cumming (2004) suggested that the relatively high accretion rate in IPs may suppress the magnetic field by overcoming ohmic diffusion, such that magnetic flux is advected into the interior of the WD. This would cause the surface magnetic field to appear less than it really is. Considering the evolution of non-magnetic CVs, i.e. the orbital period decreases until ~ 3 hr when the accretion effectively ‘turns off’ then it resumes at ~ 2 hr, allows a regime where an IP may have its ‘true’ magnetic field resurface when the accretion turns off, allow synchronization, then reappear as a polar when the accretion resumes at a lower rate. This theory also ties in with studies of isolated WDs, where peak magnetic fields of $\sim 10^9$ G are seen, whereas in binaries the field strength is typically an order of magnitude smaller (the maximum seen is 230 MG in AR UMa (Schmidt et al. 1996)) (Wickramasinghe & Ferrario 2000).

In order to test any evolutionary hypotheses an accurate determination of the magnetic fields present in IPs is needed. The best way of doing this is via circular polarization measurements.

Here we report the first paper in our survey of circular polarization emission from IPs. Initially we summarise the field as it stands, in order to put our survey in context (Sec. 2). Then we outline the method we use and the style of reporting our data (Sec. 3). Then we report the results of each of the targets (Sec. 4), followed by a discussion of each (Sec. 5). We have further data in hand for some of the Southern Hemisphere targets that we will be reporting in the near future.

2. Circular polarization

2.1. mCVs

In an accretion column in a mCV there will be material accreting onto the magnetic poles of the WD. The electrons in this material will spiral along the magnetic field lines as they fall to the surface, emitting circularly polarized radiation. The inhomogeneity of the magnetic field structure, the velocity of the electrons, and their varying temperature will have the effect of causing the electrons to emit a broad harmonic structure. By modelling the polarized radiation given off (i.e. simulating the harmonic structure) it is possible to estimate the magnetic field strength of the WD. Wickramasinghe & Meggitt (1985) did this for a range of magnetic field strengths in polars. Their models take into account the magnetic field strength, the temperature, the plasma parameter, and the viewing angle. These four variables cause the modelling to give non-unique solutions for the fitting of the harmonic curve. Their model has been used extensively in estimating the magnetic field strength in polars by measuring the level of circular polarization in different wave-bands (see e.g. Pirola et al. (1987a,b); Katajainen et al. (2003)) and has also been used in IPs (see e.g. Pirola et al. (1993)).

The polarized light measured in mCVs is generally quoted as a fraction of the total incoming radiation. In polars the source of the unpolarized and polarized radiation should vary at the same period - the orbital period. In IPs however, the situation is more complex. The presence of an accretion disc, that emits at optical frequencies, will dilute the measured polarization. If the flux from the accretion disc varies at any period other than the spin period then this will dilute the signal in a complex fashion. Added to this are the possible presence of a hot spot and the emission from the secondary which will vary at the orbital period.

The geometry of the accretion column is also an issue, since the circular polarization is not given off in all directions (see e.g. Norton et al. (2002)). The specific size/shape of the accretion column will therefore affect the emission.

Another likely complexity is that the magnetic field structure of the WD may not be dipole-like. This could lead to multiple accretion columns at multiple magnetic poles. If the magnetic field is close to being a dipole it is also possible that it could be offset from the centre, leading to one pole appearing to be stronger than the other and not at diametrically opposed poles. This complexity is further confounded by the very fact that the accreting material does not come from infinity, in which case even an ideal dipole would not form an accretion column at exactly the position of the magnetic poles.

Given all these complications we cannot be certain what the average magnetic field strength *really* is in IPs, it is possible that estimates of the field strength are over an order of magnitude understated. What we are then assuming to be low number harmonics of a low magnetic field may be high number harmonics of a much larger field.

2.2. Method of circular polarization detections

Assuming circular polarization in IPs can be measured in a similar way to polars and that IPs are of a comparable field strength, implies that harmonics will be present in the UV-IR. The optimal method to reveal these harmonics would be spin phase resolved circular spectro-polarimetry. This requires very large telescopes with very specialised instrumentation allowing high time resolution data collection. This is beyond the scope of this study, therefore we concentrate on the more readily available technique of circular photo-polarimetry.

The general principle of circular photo-polarimetry is to measure the fraction of polarized radiation after a $\lambda/4$ wave plate, which converts circular polarization into linear polarization. This process introduces biases however, for example, incomplete 90° retardation by the wave plate. These biases may cause so called ‘Stokes parameters cross talks’, particularly in the case of targets with non-negligible linear polarization. These cross talks can effectively be eliminated by rotating the wave plate to at least two different wave plate angles and then calculating a single measurement of the circular polarization by using flux values from both positions. This process has an important effect on the temporal resolution of the data, since enough time must be spent integrating on the target to get a good signal to noise value, and if this has to be done multiple times then the temporal resolution will suffer.

By taking simultaneous circular polarization measurements in different pass-bands a clearer understanding of the harmonic structure may be gained. If the pass-bands are defined to have a range comparable to the expected width of the harmonics then comparison of the circular polarization in each band gives an indication of the magnetic field strength.

The method of reporting the level of circular polarization is rather ambiguous, some authors quote the average level throughout their observing run (e.g. Stockman et al. (1992)), some give orbitally binned data, but most report data phase binned at the spin period. Each method may have the effect of giving a different interpretation of the magnetic field (see e.g. Uslenghi et al. (2001) where the data is presented in mean, spin binned and orbitally binned format). The average value approach could potentially smooth a sinusoidal-like variation, with an arbitrary amplitude and zero offset, to an average of zero. Phase binning at the orbital period may be severely affected by the variation in orbitally varying unpolarized light. Phase binning over the spin period can reduce both these effects, and since the circular polarization is thought to originate from the accretion column (emission from which varies at the spin period) this is therefore the most desirable approach. The base line chosen needs to be sympathetic to the orbital variation, i.e. either be short in relation to the orbital period, or considered in chunks, and the integration time short compared to the spin period.

2.3. Previous Circular polarization detections in IPs

DQ Her was the first IP (although not classified as an IP at the time) to have circular polarization detected (Swedlund et al. 1974). This white light detection was carried out over the course of three months allowing many measurements over the entire 4.6 hr orbital period. The level of circular polarization was found to vary periodically over the spin period (142 s) and to be both positive and negative. This variation was found to have a different profile over the orbital period also. The maximum amplitude of variation was found to be approximately 0.6%. Stockman et al. (1992) also measured the level of circular polarization on DQ Her, they found a mean level of $+0.01 \pm 0.01\%$, however, they remark that short period systems will have their levels of reported circular polarization reduced due to the long measurement times.

The next detection of circular polarization in an IP was BG CMi (Penning et al. 1986; West et al. 1987). Measurements were taken in five different pass bands at various times over four months. This allowed the measurements to be plotted over the orbital period (3.75 hr). In the $1.10 - 1.38\mu\text{m}$ band the data were distributed randomly about the mean of $-1.74 \pm 0.26\%$ indicating no orbital modulation. Phase binning the data at the spin period (15.9 min) showed a coherent modulation, however the variation was within two sigma of being zero. West et al. (1987) also considered the variation of the circular polarization with the passband, they found that the amplitude detected increased with wavelength, ranging from $-0.053 \pm 0.051\%$ at $0.32 - 0.86\mu\text{m}$ to $-4.24 \pm 1.78\%$ at $1.40 - 1.65\mu\text{m}$.

PQ Gem (RE 0751+14) was found in the early 1990's to exhibit significant circular polarization which was modulated at the spin period (Rosen et al. 1993; Piirola et al. 1993; Potter et al. 1997).

Since then, several IPs have been found to exhibit similar behaviour, or have had upper limits placed on their circular polarization (see Table 1 for a summary of all measurements).

V2306 Cyg is the only reported IP to show significant positive polarization in one band and negative in another (Norton et al. 2002), this requires two opposite poles to be seen and for them to be in different states (i.e. one or more of the temperature, geometry, accretion rate etc must be different at the two poles). In all the other cases the polarization has the same sign across the different wave bands.

Table 2. Inferred magnetic field strengths from the measured circular polarization in IPs.

Name	Inferred magnetic field strength (MG)	Reference
BG CMi	5–10	West et al. (1987)
	3–10	Chanmugam et al. (1990)
PQ Gem	8–18	Piirola et al. (1993)
	9–21	Vaeth et al. (1996)
	9–21	Potter et al. (1997)
V2400 Oph	8	Buckley et al. (1995)
	9–27	Vaeth (1997)
V405 Aur	~ 30	Piirola et al. (2008)

Each significant (non-zero) measurement of circular polarization has had an estimate of the magnetic field present on the WD attributed to it. Different approaches to modelling the emission have lead to differing inferred values however (see Table 2).

Given the rather disparate nature of previous studies, which generally tend to have information lost in the style of reporting, we have initiated a survey to conclusively measure the degree of circular polarization and comprehensively characterise its nature in IPs.

3. Observations

Observations were carried out at the 2.56m Nordic Optical Telescope (NOT) on the island of La Palma over three consecutive nights starting 2006 July 31. The telescope was fitted with the TurPol instrument. This is the double image chopping polarimeter (Piirola 1973, 1988; Korhonen et al. 1984), which is able to perform simultaneous photo-polarimetric measurements in all *UBVRI* bands, by using four dichroic filters (which split the light into five spectral pass-bands). The pass-bands are defined as having an effective wavelength of 360, 440, 530, 690, and 830 nm for each of *UBVRI* respectively. By inserting a plane parallel calcite plate into the beam before the focal plane, polarization measurements are possible. The calcite splits the incoming light into two components, the ordinary and the extra-ordinary, which are orthogonally linearly polarized. A diaphragm in the instrument has two apertures, one passes the star's ordinary component, the other passes the extra-ordinary component. A chopper opens and closes the apertures alternately, illuminating the photo-cathode of the photomultiplier tube. By measuring the relative intensities of components after a wave-plate, (which may be rotated in 90° steps) the degree of circular polarization of the light entering from the star can be calculated. Both components of the sky background pass both diaphragms, and the polarization of the sky is thus directly eliminated. In addition, measurements of empty sky are also done at 10 minute intervals, as this sky value is needed in calibration of the photometry.

For one polarization data point, normally at least four multiples of the integration time plus mechanical dead-time (few seconds) generated from rotation of the wave plate is needed, assuming that the circular polarization is measured from two different wave plate positions. This will have the effect of 'smearing' out the data on some very short period objects, and therefore may under report their true polarization value. In this study, as some of the targets show remarkable variability within a short timescale, we have chosen in those cases to use only one wave plate position measurement, instead of two. The reduction software was altered in such a way that it could take a circular polarization measurement from only one position of the wave plate.

Table 3. Target list.

Name	α 2000	δ 2000	V (mag)	P _{spin} (s)	P _{orb} (h)
RXJ1730	17:30:21	−05:59:32	15.8	128.0	15.42
DQ Her	18:07:30	+45:51:32	13	142.1	4.65
V1223 Sgr	18:55:02	−31:09:48	13.2	745.6	3.37
V2306 Cyg	19:58:14	+32:32:42	16	1466.7	4.35
AE Aqr	20:40:09	−00:52:16	12	33.1	9.88
RXJ2133	21:33:44	+51:07:24	15.3	570.8	7.19
FO Aqr	22:15:55	−08:21:05	13.5	1254.5	4.85
AO Psc	22:55:17	−03:10:39	13.3	805.2	3.59
RXJ1730 = 1RXS J173021.5−055933,					
RXJ2133 = 1RXS J213344.1+510725.					

Table 5. Calibration data (taken on the first night).

Band	Instrumental polarization		Measured standard polarization	
	Value (%)	uncertainty (%)	Value (%)	uncertainty (%)
<i>U</i>	−0.005	0.030	+0.126	0.103
<i>B</i>	−0.064	0.024	−3.607	0.112
<i>V</i>	−0.017	0.028	−3.959	0.166
<i>R</i>	−0.011	0.024	−4.064	0.156
<i>I</i>	−0.059	0.029	−2.647	0.226

This single position polarization measurement improves the temporal resolution of the data, but at the cost of increasing the uncertainty on the measurement as the biases are not cancelled out.

The targets chosen for this northern hemisphere survey are those in Table 3, and the observing log in Table 4. Note the very short period systems (AE Aqr (33 s), DQ Her (142 s), and RX1730 (128 s)) have one orientation of the wave-plate per measurement, and the other targets have two.

The instrumental polarization was small in all bands (see Table 5). The circular polarization standard star GRW+70 8247 (West 1989) was used to check the calibration, the values reported here are consistent with previous measurements of the standard. The uncertainties quoted on each circular polarization measurement are based on photon noise and are one sigma.

The zero points of the *UBVRI* magnitude scale were determined by observations of Landolt standards (109 954, 111 250, 111 2093 and 114 637; Landolt (1992)) during each night.

4. Results

Successful measurements are outlined for seven of the targets below. The results of RXJ2133 are reported separately in Katajainen et al. (2007).

Given the ambiguity in the previously reported results, we give our data in multiple formats. The average value over the run will show any large unmodulated polarization (like that in BG CMi) and allow comparison with most of the previous measurements. The peak amplitude (of the spin folded and phase binned data) gives an idea of how modulated the system is. The peak to peak value shows whether or not both magnetic poles can be seen, and gives the best indication of the presence of modulation.

4.1. AE Aqr

AE Aqr has the shortest spin period of all the known IPs (~ 33 s), and a relatively long orbital period of 9.88 h. Observed over

two nights it was at an orbital phase of 0.6 and 0.3 from superior conjunction of the WD with respect to the secondary on the two nights respectively (Welsh et al. 1993). We used a spin period of 0.000382833 d, calculated for July/August 2006 from the ephemeris of de Jager et al. (1994). The zero spin phase point used here is arbitrarily set to the midnight epoch at HJD 2 453 949.5.

Over the two nights this system showed a marked difference in its behaviour. During the first night the *U* band exhibited significant flickering and a general trend of an increase in magnitude (see Fig. 1). This was mirrored in the raw *U* band circular polarization where the magnitude increased as the run went on. On the second night the *U* band exhibited significantly less flickering. This was a trend that was seen in all bands to some extent (see Fig. 1). This flickering is a well known feature of AE Aqr (see e.g. Beskrovnyaya et al. (1996)). With this in mind the data from the two nights is presented separately.

The short period of the system is such that the temporal resolution must be as small as possible to search for any periodic variations. In order to satisfy this only one position of the wave plate was used for each polarization measurement. On the first night an integration time of ~ 3 s was used, this gave an overall temporal resolution of ~ 8.5 s. On the second night an integration time of ~ 1 s was used, giving a temporal resolution of ~ 4.5 s for a full polarization measurement. Even at this short time scale the measurements will be smoothed to some extent. The data was folded and binned into 10 bins over the spin cycle (see Figs. 2 and 3). Both nights show a very small amplitude circular polarization. However in the raw data, values with an amplitude of over 2% (with a typical error of 0.6%) are not uncommon.

The mean values in each band (over each of the nights) are all within three sigma of zero. The peak amplitude is $0.80 \pm 0.39\%$ and the maximum peak to peak value is $1.22 \pm 0.48\%$ (see Table 6). The short spin period means that this data set covers many spin periods, and therefore the signal to noise is good.

4.2. AO Psc

AO Psc is a typical IP with a spin and orbital period of 805.2 s and 3.59 h respectively. Using the orbital ephemeris of Kaluzny & Semeniuk (1988), AO Psc was at an orbital phase of 0.14 from the maximum optical light. We note that the error in the calculation of this phase is small, but the ephemeris is old (20 years) so it may be somewhat out of date. The spin ephemeris has an accumulated uncertainty of greater than one spin, so we have used a zero point of HJD 2 453 949.5. The spin period from Kaluzny & Semeniuk (1988) of 0.0009319484 d was used.

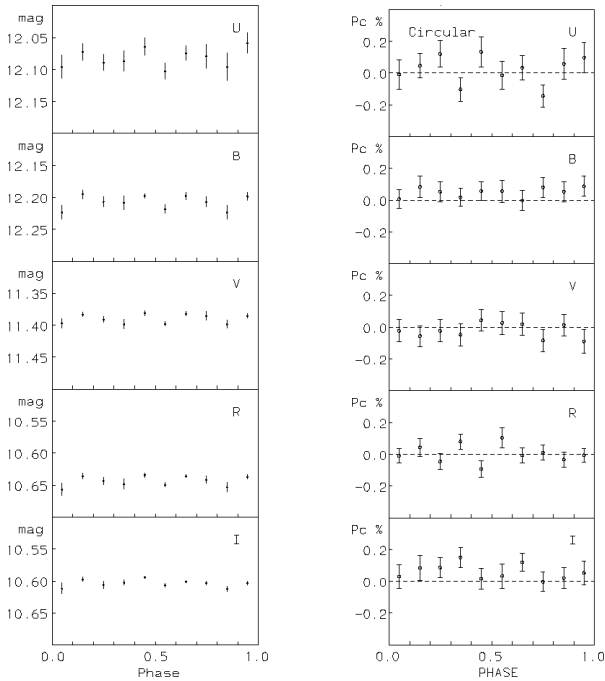
Each polarization measurement consisted of two positions of the wave plate at 10 s each. The polarization data was then binned into eight bins across the spin cycle. The mean values in each band were within three sigma of being zero. The maximum amplitude in the binned data was $0.86 \pm 0.37\%$, with a maximum peak to peak variation of $1.30 \pm 0.50\%$, see Fig. 4 and Table 6. This peak to peak variation is less than three sigma, so we cannot claim this as a reliable detection of variable polarization.

4.3. DQ Her

DQ Her has an orbital period of 4.65 h and a spin period of 142 s. Using the ephemerids of Zhang et al. (1995) DQ Her was at an orbital phase of 0.23 from the optical eclipse. We used an

Table 4. Observing log.

Name	Start time (HJD ^a)	End time (HJD ^a)	Duration (mins)	No. of P _{orb}	No. of P _{spin}	Filters	Exposure time ^b (s)	Resolution ^c (s)	V ^d (mag)
DQ Her	13 948.4240	13 948.5349	159.7	0.57	67.4	UBVRI	1 × 10	~ 24	14.5
RXJ2133	13 948.5732	13 948.6542	116.6	0.27	12.3	UBVRI	4 × 10	~ 96	15.3
FO Aqr	13 948.6933	13 948.7091	22.8	0.08	1.1 ^e	UBVRI	2 × 10	~ 48	13.9
AE Aqr	13 949.5103	13 949.5704	86.5	0.15	156.8	UBVRI	1 × 3	~ 8.5	11.4
V2306 Cyg	13 949.5794	13 949.6528	105.7	0.40	4.3	UBVRI	2 × 10	~ 48	14.7
AO Psc	13 949.7047	13 949.7194	21.2	0.10	1.6 ^e	UBVRI	2 × 10	~ 48	13.2
RXJ1730	13 950.4112	13 950.5134	147.2	0.16	69.0	UBVRI	1 × 10	~ 24	16.3
V1223 Sgr	13 950.5298	13 950.5871	82.5	0.41	6.6	UBVRI	2 × 10	~ 48	13.7
AE Aqr	13 950.6224	13 950.6366	20.4	0.03	37.0	UBVRI	1 × 1	~ 4.5	11.6
RXJ2133	13 950.6455	13 950.7187	105.4	0.24	11.1	UBVRI	4 × 10	~ 96	15.2

^a +2 440 000^b The number of orientations of the wave plate, and the time spent at each orientation.^c The resolution is roughly the number of orientations of the wave plate multiplied by the exposure time multiplied by two (to account for the ordinary and extraordinary measurements) plus some mechanical dead time.^d Measured.^e These data sets are short and therefore the reported uncertainties are probably underestimated.**Fig. 2.** Spin folded and phase binned simultaneous *UBVRI* photometry (left) and circular polarization (right) plots of AE Aqr, taken on the first night (HJD 2 453 949). Zero phase corresponds to HJD 2 453 949.5. A spin period of 0.000382833 d was used.

arbitrary zero point of phase as HJD 2 453 948.5. A spin value of 0.00164504 d was used.

Due to the short period, a single wave plate position was used for an integration time of 10 s. The data was binned into ten bins over the spin period. All of the mean polarization values are less than three sigma from zero. The maximum amplitude seen is $0.64 \pm 0.31\%$ and the maximum peak to peak value was $1.00 \pm 0.39\%$ (see Table 6), this is less than a three sigma detection of variation (see Fig. 5).

4.4. FO Aqr

FO Aqr has an orbital period of 4.85 h and a spin period of 1254.5 s. Using the ephemeris of Patterson et al. (1998), FO Aqr

was at an orbital phase of 0.98 from the dip in the optical light curve at the start of this observation. It was also at a spin phase of approximately 0.6 from pulse maximum, but we note that FO Aqr is rather erratic and this value may be some way off now, so zero phase was arbitrarily set to HJD 2 453 948.5. Here a spin value of 0.014519035 d from Patterson et al. (1998) was used.

Each polarization measurement was taken with two positions of the wave plate with an integration time of 10 s in each. The data was binned into four bins over the spin cycle. The mean circular polarization was within two sigma of being zero in each band. A peak amplitude of $1.15 \pm 0.65\%$ is present in the *I* band (see Fig. 6). The peak to peak values had a maximum of $1.43 \pm 0.80\%$ (see Table 6).

4.5. 1RXS J173021.5–055933

1RXS J173021.5–055933 (RXJ1730) is a relatively newly classified IP. It has a reported orbital period of 15.42 hr and spin period of 128.0 s (Gänsicke et al. 2005). This short period (and therefore large number of spin cycles) has rendered the spin ephemeris of de Martino et al. (2008) out of date, and there is no published orbital ephemeris. Zero spin phase was set to HJD 2 453 950.5. A spin period of 0.001481481 d (Gänsicke et al. 2005) was used.

Here the first simultaneous *UBVRI* photometry of this object is presented (see Fig. 7). The photometry exhibits a double peak profile with equal maxima and unequal minima in each band. The photometric CLEANED (Lehto 1997) periodograms of each individual band are shown in Fig. 8. The spin period is seen at a value of 128.1 ± 0.7 s and the first harmonic at 64.0 ± 0.2 s (uncertainties based on a one sigma Gaussian fit to the periodogram). The spin peak is seen strongest in the *V* band.

The wave plate was positioned in one orientation for each circular polarization measurement for 10 s. The data were binned into 15 bins over the spin cycle. In each band the mean circular polarization was within two sigma of being zero. The biggest amplitude modulation was $4.26 \pm 1.09\%$ and the greatest peak to peak value was $8.26 \pm 1.56\%$ (see Table 6). The spin period was recovered from a period search of the *B* band circular polarization also. The short spin period means that many spin cycles (69) were completed, this leads to a high confidence in this data set.

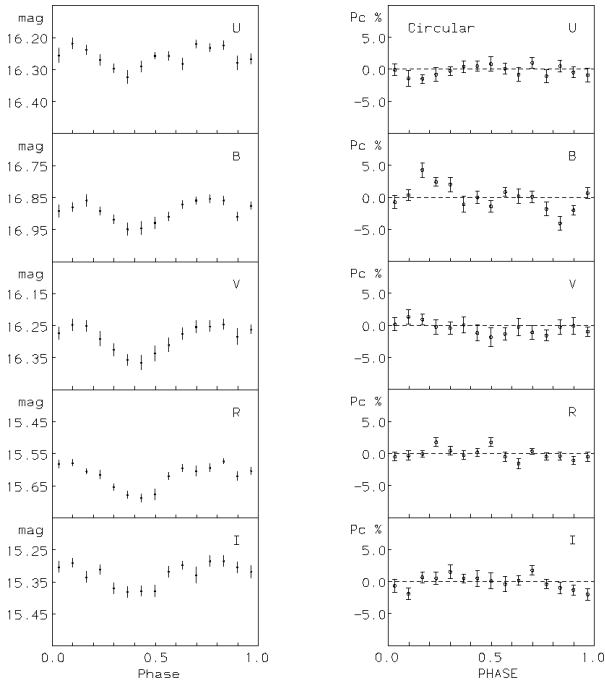


Fig. 7. Spin folded and phase binned simultaneous *UBVR* photometry (left) and circular polarization (right) plots of RXJ1730. Zero phase corresponds to HJD 2453950.5. A spin period of 0.001481481 d was used.

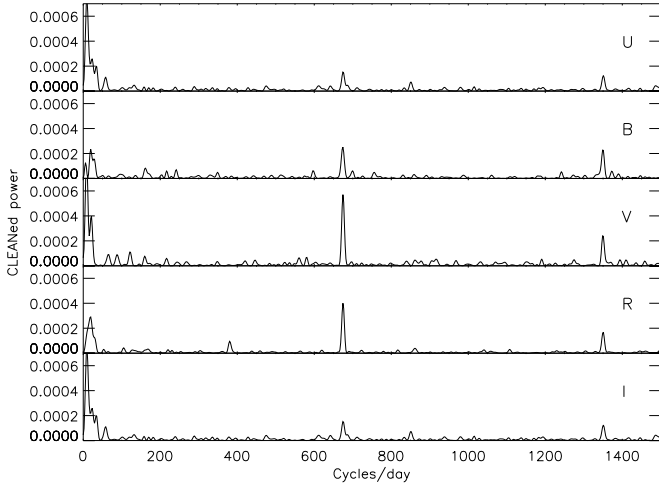


Fig. 8. *UBVR* CLEANED photometric periodograms of RXJ1730.

4.6. V1223 Sgr

V1223 Sgr has a spin and orbital period of 745.6 s and 3.37 h respectively. Using the orbital ephemeris of Jablonski & Steiner (1987) V1223 Sgr is at an orbital phase of 0.83 from the maximum light, again this phase is valid with respect to the ephemeris, but the ephemeris is over 20 years old. The spin ephemeris has accumulated too much uncertainty to be useful here, so zero phase was arbitrarily set to HJD 2453950.5. A spin value of 0.00863 d from Osborne et al. (1985) was used.

The polarization measurements consisted of two positions of the wave plate, each of 10 s. The data was binned into ten bins across the spin cycle. The mean values of the circular polarization are all within three sigma of being zero. The maximum amplitude variation was $1.30 \pm 1.12\%$ in the *U* band and the maximum peak to peak value was $2.16 \pm 1.22\%$ (see Fig. 9). The

peak to peak values are all within three sigma of being zero (see Table 6).

4.7. V2306 Cyg

V2306 Cyg has an orbital period of 4.35 h and a spin period of 1466.7 s (Norton et al. 2002; Zharikov et al. 2002). The spin ephemeris of Norton et al. (2002) was used to phase the spin variations here.

Each polarization measurement consisted of two positions of the wave plate, each position being 10 s. The data were binned into 15 bins over the spin cycle. The maximum amplitude circular polarization was $1.06 \pm 0.41\%$ in the *I* band. The mean circular polarization in each band is consistent with zero (see Table 6). The maximum peak to peak value ($1.95 \pm 0.66\%$ in the *I* band) indicates that variation is present (see Fig. 10 and Table 6).

4.8. Summary of results

Table 6 summarises the results obtained, this should now be used in conjunction with the results in Table 1. As noted earlier, our results on RXJ2133 have been reported separately in Katajainen et al (2007).

5. Discussion

5.1. AE Aqr

This is the first simultaneous *UBVR* polarimetry measurement of AE Aqr. In most previous measurements a broad band filter and/or a much too long integration time has been used (see Table 1). This will have had the effect of smearing any polarization out to almost zero. In the cases where a short integration time has been used only a mean value has been reported, except for Cropper (1986) where a maximum semi-amplitude of $\sim 0.1\%$ was given.

The data reported here broadly agrees with the previous mean measurements of close to zero. The small peak to peak values are also in agreement with this. We do note that there is a hint of circular polarization in the raw data (over 2% in places - with a typical error of 0.6%).

Given the generally accepted view that AE Aqr is a propeller system it seems intuitive to assume that it would have a large magnetic field to power this regime. Norton et al. (2008) have shown in their theoretical modelling that propellers can exist at low magnetic field strengths when they are spinning sufficiently fast. So a large magnetic field in AE Aqr is not necessarily required.

5.2. AO Psc

This is the first simultaneous *UBVR* polarimetric observation of this target. All previous measurements have had a long integration time (≥ 240 s) when compared to the spin period (805.2 s) (see Table 1), so any variations shorter than this will have been smeared out effectively.

The mean measured circular polarization values are consistent with previous measurements (all of which were within one sigma of zero) (see Table 1).

The peak to peak values show hints of variation, ($1.30 \pm 0.50\%$) in the *I* band, but the detection is not conclusive. The short data set (1.6 spin periods) means that the uncertainties in this observation are large. This, coupled with the non-zero peak

Table 6. Summary of results. Min and max correspond to the phase binned data.

Target	Filter	Mean (%)	Min (%)	Max (%)	Peak-Peak (%)
AE Aqr ^a	<i>U</i>	+0.02 ± 0.02	-0.14 ± 0.07	+0.13 ± 0.10	0.27 ± 0.12
	<i>B</i>	+0.05 ± 0.02	-0.00 ± 0.06	+0.09 ± 0.06	0.09 ± 0.08
	<i>V</i>	-0.02 ± 0.02	-0.09 ± 0.08	+0.04 ± 0.07	0.13 ± 0.11
	<i>R</i>	+0.01 ± 0.01	-0.09 ± 0.05	+0.11 ± 0.06	0.20 ± 0.08
	<i>I</i>	+0.06 ± 0.02	-0.00 ± 0.06	+0.15 ± 0.07	0.15 ± 0.09
AE Aqr ^b	<i>U</i>	+0.00 ± 0.08	-0.27 ± 0.26	+0.38 ± 0.23	0.65 ± 0.35
	<i>B</i>	-0.07 ± 0.07	-0.46 ± 0.21	+0.26 ± 0.21	0.72 ± 0.30
	<i>V</i>	+0.08 ± 0.07	-0.33 ± 0.23	+0.50 ± 0.26	0.83 ± 0.35
	<i>R</i>	+0.02 ± 0.04	-0.14 ± 0.18	+0.34 ± 0.18	0.48 ± 0.25
	<i>I</i>	+0.10 ± 0.07	-0.42 ± 0.28	+0.80 ± 0.39	1.22 ± 0.48
AO Psc	<i>U</i>	+0.07 ± 0.05	-0.06 ± 0.14	+0.48 ± 0.16	0.54 ± 0.21
	<i>B</i>	+0.07 ± 0.06	-0.08 ± 0.20	+0.20 ± 0.28	0.28 ± 0.34
	<i>V</i>	+0.05 ± 0.09	-0.55 ± 0.33	+0.43 ± 0.25	0.98 ± 0.41
	<i>R</i>	-0.02 ± 0.08	-0.44 ± 0.29	+0.19 ± 0.21	0.63 ± 0.36
	<i>I</i>	+0.29 ± 0.10	-0.44 ± 0.35	+0.86 ± 0.37	1.30 ± 0.50
DQ Her	<i>U</i>	+0.00 ± 0.04	-0.16 ± 0.14	+0.19 ± 0.13	0.35 ± 0.19
	<i>B</i>	+0.14 ± 0.05	-0.05 ± 0.17	+0.47 ± 0.16	0.53 ± 0.23
	<i>V</i>	+0.12 ± 0.07	-0.08 ± 0.25	+0.35 ± 0.29	0.43 ± 0.39
	<i>R</i>	+0.03 ± 0.06	-0.22 ± 0.20	+0.40 ± 0.23	0.61 ± 0.31
	<i>I</i>	+0.04 ± 0.07	-0.64 ± 0.31	+0.35 ± 0.25	1.00 ± 0.39
FO Aqr	<i>U</i>	+0.16 ± 0.10	-0.00 ± 0.24	+0.56 ± 0.53	0.60 ± 0.58
	<i>B</i>	+0.07 ± 0.10	-0.27 ± 0.20	+0.47 ± 0.28	0.74 ± 0.34
	<i>V</i>	+0.17 ± 0.15	-0.38 ± 0.36	+0.40 ± 0.36	0.78 ± 0.51
	<i>R</i>	+0.11 ± 0.12	-0.01 ± 0.60	+0.42 ± 0.30	0.43 ± 0.67
	<i>I</i>	+0.27 ± 0.20	-0.28 ± 0.47	+1.15 ± 0.65	1.43 ± 0.80
RXJ1730	<i>U</i>	-0.23 ± 0.18	-1.48 ± 0.72	+1.02 ± 0.84	2.50 ± 1.11
	<i>B</i>	+0.00 ± 0.21	-4.00 ± 1.11	+4.26 ± 1.09	8.26 ± 1.56
	<i>V</i>	-0.39 ± 0.21	-1.79 ± 1.45	+1.38 ± 1.19	3.17 ± 1.88
	<i>R</i>	-0.07 ± 0.13	-1.55 ± 0.79	+1.80 ± 0.67	3.35 ± 1.07
	<i>I</i>	-0.12 ± 0.19	-1.95 ± 0.93	+1.82 ± 0.75	3.77 ± 1.19
V1223 Sgr	<i>U</i>	-0.01 ± 0.20	-1.30 ± 1.12	+0.86 ± 0.48	2.16 ± 1.22
	<i>B</i>	-0.00 ± 0.08	-0.40 ± 0.34	+0.36 ± 0.38	0.77 ± 0.51
	<i>V</i>	-0.04 ± 0.09	-0.45 ± 0.25	+0.55 ± 0.41	1.00 ± 0.48
	<i>R</i>	-0.05 ± 0.09	-0.40 ± 0.36	+0.32 ± 0.55	0.71 ± 0.65
	<i>I</i>	-0.27 ± 0.11	-0.92 ± 0.43	+0.50 ± 0.46	1.42 ± 0.63
V2306 Cyg	<i>U</i>	+0.06 ± 0.08	-0.61 ± 0.45	+0.61 ± 0.33	1.23 ± 0.56
	<i>B</i>	-0.00 ± 0.07	-0.47 ± 0.51	+0.46 ± 0.29	0.92 ± 0.59
	<i>V</i>	-0.07 ± 0.08	-0.86 ± 0.29	+0.51 ± 0.37	1.36 ± 0.48
	<i>R</i>	-0.08 ± 0.06	-0.78 ± 0.26	+0.45 ± 0.26	1.23 ± 0.37
	<i>I</i>	-0.11 ± 0.10	-1.06 ± 0.41	+0.89 ± 0.52	1.95 ± 0.66

^a First night; ^b Second night.

to peak values and a tentative detection in the *I* band may warrant further investigation.

5.3. DQ Her

This is the first simultaneous *UBVRI* polarimetric observation of DQ Her. The maximum level of circular polarization seen here ($0.64 \pm 0.31\%$) is consistent with the plots of Swedlund et al. (1974) who illustrate a variation with a max/min of $\geq 0.5\%$. They found that the polarization was also variable on the orbital period, our data was just under 0.6 of a complete orbital period so we cannot bin our data as they did, and we see no overall trend in our data. Their pass band was approximately equal to our *UBV* bands combined.

The only other measurement of circular polarization in DQ Her was that of Stockman et al. (1992). They give a broadband integrated result close to zero, this is likely consistent with Swedlund et al. (1974) who see both positive and negative polarization values. As such, this is the first published result of time-resolved *R* and *I* band (as well as the first simultaneous *UBVRI*)

data. The largest departure from zero polarization is seen in the *I* band here, and the raw data show up to $6 \pm 1\%$.

Although by itself this data cannot claim a significant circular polarization detection, when considered with the results of Swedlund et al. (1974), it seems likely that DQ Her does exhibit variable circular polarization. To make a definite conclusion, more measurements are needed, particularly in the *I* band.

5.4. FO Aqr

This is the first simultaneous *UBVRI* polarimetry of FO Aqr. All previous measurements report a mean value close to zero, except for in the $1.15 - 1.35\mu\text{m}$ range where $+1.1 \pm 0.3\%$ polarization has been detected (see Table 1). The mean circular polarization seen here is within two sigma of all the previous measurements where there is an overlap in pass band (see Table 1). Since the large value of the circular polarization in the *I* band has such a large uncertainty we cannot claim this as a detection, although it is possible that circular polarization is present at the level of around 1%.

The short data set (1.1 spin periods) means that the uncertainties are probably much higher than quoted. This system also perhaps warrants further investigation, particularly in the *I* band.

5.5. RXJ1730

RXJ1730's short spin period (128.0 s) and long orbital period (15.4 hr) make it a close sibling to the enigmatic AE Aqr (spin and orbital periods of 33.1 s and 9.88 h respectively).

The photometric data shows a double peaked profile with equal maxima and unequal minima (see Fig. 7). Period analysis yields a spin period of 128.1 ± 0.7 with the first harmonic visible at 64.0 ± 0.2 s. This is in good agreement with Gänsicke et al. (2005) who concluded that both poles could be seen.

de Martino et al. (2008) report simultaneous optical Sloan filter data from the *u'*, *g'* and *r'* bands. The *u'* filter is approximately the same as our *U* band, *g'* covers all our *B* and the upper half of *V*, and *r'* covers the lower half of *V* as well as *R*. In each of their *u'*, *g'* and *r'* band observations the fundamental and the first harmonic were seen, with the first harmonic, on average, being strongest. This is in contrast to what we see (see Fig. 8), i.e. the fundamental being dominant. However, de Martino et al. (2008) show their *r'* band power spectra obtained on each of six consecutive nights. This shows a marked change in the relative strengths of the first harmonic and fundamental over time, the last night exhibiting a similar structure to ours. de Martino et al. (2008) see the strongest signal in their *g'* and *u'* bands, our *U* band has very little power, but our *V* band is the strongest, and since this contributes to what is their *g'* band this tallies up.

The level of polarization, $8.26 \pm 1.56\%$ peak to peak in the *B* band, makes this one of the most variable circularly polarized IPs, and therefore likely one of the most magnetic, measured to date. The variation of the circular polarization in the *B* band, showing both positive and negative values is indicative of both magnetic poles being visible (since each pole may only emit either positive or negative circular polarization). We note that the raw circular polarization data is somewhat noisy, with individual measurements of over 15%, we are unsure of the origin of these values, but we speculate that they may arise from short epochs when the diluting light is randomly lower due to flickering.

In the *B* band the photometry and circular polarization are coincident; the peaks in the photometry align with the peak and trough in the circular polarization. This strengthens the assertion that both poles are seen and they are both emitting circular polarization.

Like many of the other IPs for which circular polarization has been detected, RXJ1730 is also an *INTEGRAL* source (Barlow et al. 2006). We discuss this further in Section 5.8.

The variable nature of this object over the course of several days (de Martino et al. 2008) makes this an ideal target for a long base line follow up. Monitoring how the circular polarization varies as the accretion column structure changes over time and linking this to the photometry may reveal more about the magnetic nature of this source and IPs in general. Phase resolved circular spectro-polarimetry would be the ideal tool in revealing the magnetic field strength of RXJ1730, but taking into account the extremely short spin period (128 s), and relative faintness ($V \sim 17$) there are very few telescope and instrument combinations available where these kind of observations are possible.

5.6. V1223 Sgr

The mean circular polarization in V1223 Sgr is within four sigma of the previously reported values, and zero (see Tables 1 & 6). The maximum peak to peak variation of $2.16 \pm 1.22\%$ in the *U* band is not constrained enough for this to be considered a definite detection, but when considered with the results of Watts et al. (1985) it is likely that V1223 Sgr is strongly polarized.

There is a clear hint of a double peaked structure in the *UVRI* circular polarization curves, indicating that two magnetic poles can be seen. This is an effect seen in the photometry also, with hints of a double peaked profile in each band. This is in contrast to previous results which show a single peaked structure.

The raw circular polarization measurements are stable in all bands at the start of the run, but the *U* band begins to fluctuate as the run goes on, sometimes, quite randomly, up to 20%.

V1223 Sgr has a similar spin and orbital period to V405 Aur which was recently found to be very magnetic (Piirola et al. 2008) and has its circular polarization peak in the blue part of the spectrum. If the level of polarization seen here is confirmed then V1223 Sgr would be a close twin of V405 Aur. We also note that V1223 Sgr is an *INTEGRAL* source (Barlow et al. 2006).

5.7. V2306 Cyg

V2306 Cyg has had significant levels of circular polarization reported previously; Uslenghi et al. (2001) first reported it after using the TurPol instrument at the NOT (results summarised in Table 1). The mean results reported here are within the bounds given by uncertainties (two sigma) in their *UBV* bands, however in *R* and *I* Uslenghi et al. (2001) find a much higher amplitude mean value. Norton et al. (2002) also reported *B* and *R* band polarization at the NOT, this time using the ALFOSC instrument, they obtained mean values of $+0.32 \pm 0.10\%$ and $-1.99 \pm 0.11\%$ in each band respectively. Here we see significantly lower values than theirs also.

The shape of the circular polarization variation seen here is one of two minima per spin cycle in the *B* and *I* bands (see Fig. 10). The *B* band of Norton et al. (2002) has an indication of a two peaked profile, our results confirm this.

The discrepancy between our results and those reported previously can be explained in a variety of ways. The orbital phase may be different during each of the observations, Uslenghi et al. (2001) showed the circular polarization varied significantly over the orbital period, unfortunately the orbital ephemeris has accumulated too much uncertainty for this to be calculated. Another consideration is the brightness of the source, Uslenghi et al. (2001) did not quote a magnitude, but Norton et al. (2002) measured *UBVRI* magnitudes which are significantly fainter than ours. Since circular polarization is calculated as a fraction of the total incoming light this may have had the effect of seriously diluting our result.

5.8. Implications of our results

Generally each of the definite or potential circular polarization detections reported here have been most prominent towards the red end of the spectrum. This is in agreement with what has been seen before, and reinforces the notion of IPs being less magnetic than polars, as weaker fields will give rise to polarization appearing at longer wavelengths.

Amongst the IPs detected by *INTEGRAL* (Barlow et al. 2006; Bird et al. 2007) RXJ2133 and V2400 Oph have pre-

viously been found to display a large degree of circular polarization (Katajainen et al. 2007; Buckley et al. 1995, 1997), whilst RXJ1730, V2306 Cyg, DQ Her, V1223 Sgr and FO Aqr are shown here to have some degree of circular polarization or at least strong hints of it. The only other *INTEGRAL*-detected IP to have its circular polarization measured is GK Per (Stockman et al. 1992). This was reported as having a mean value of $0.03 \pm 0.10\%$, but as noted earlier, the practice of reporting mean values may seriously under report the true magnetic nature. In light of this, it would be productive to look for circular polarization in the rest of the *INTEGRAL* IP sources, namely V709 Cas, IGR000234+6141, NY Lup, and MU Cam. As noted by Katajainen et al. (2007), NY Lup may well be a close twin of the strongly polarized IP RXJ2133.

It has also been noted that the presence of a soft X-ray component may be related to the presence of a large magnetic field (Katajainen et al. 2007). The circular polarization seen in RXJ1730 further adds to this trend as it is also a soft X-ray source (de Martino et al. 2008). This brings the total of soft X-ray emitting, circularly polarized IPs to four, namely PQ Gem, V405 Aur, RXJ2133 and RXJ1730. Perhaps the same geometry which allows the soft X-ray component to be seen in some IPs but not others, as suggested by Evans & Hellier (2007), may also allow the efficient detection of circular polarization. Indeed Evans & Hellier (2007) suggested that the reason some IPs show polarization and the others do not, is mostly due to different accretion geometry and hiding effects of the accretion curtains. This may tie in with the suggestion by Norton et al. (2002) with regard to V2306 Cyg, that cancellation of polarized emission between the two magnetic poles may hide significant polarization in some systems. Furthermore, it may be that only those systems which show an asymmetry between the poles (in terms of temperature etc or accretion curtain structure) or have an offset or non-dipole magnetic field structure, emit a detectable signal.

6. Conclusion

We have detected temporal variation in the circular polarization emission in RXJ1730, with possible emission (and in some cases variation) in V2306 Cyg, DQ Her, V1223 Sgr, AO Psc and FO Aqr; AE Aqr had none detected at a significant level. Broadly speaking this is in agreement with previous results, and adds to the observational trend of IPs having less polarization than polars; and hence likely smaller effective magnetic field strength.

There are indications of a correlation between the detection of circular polarization in IPs and their detection as hard X-ray sources by *INTEGRAL*. We therefore suggest that other *INTEGRAL* sources should be tested for circular polarization. Where such objects also exhibit soft X-ray components (i.e. NY Lup and MU Cam), we predict there is a very good chance of detecting significant circular polarization.

7. Acknowledgements

The Nordic Optical Telescope is operated on the island of La Palma jointly by Denmark, Finland, Iceland, Norway, and Sweden, in the Spanish Observatorio del Roque de los Muchachos of the Instituto de Astrofísica de Canarias. This work has been supported by the “Societas Scientiarum Fennica - Suomen Tiedeseura” and its Magnus Ehrnrooth foundation, and the Academy of Finland (SK).

References

- Barlow, E. J., Knigge, C., Bird, A. J., et al. 2006, *MNRAS*, 372, 224
 Berriman, G., Bailey, J., Axon, D. J., & Hough, J. H. 1986, *MNRAS*, 223, 449
 Beskrovnaya, N. G., Ikhsanov, N. R., Bruch, A., & Shakhovskoy, N. M. 1996, *A&A*, 307, 840
 Bird, A. J., Malizia, A., Bazzano, A., et al. 2007, *VizieR Online Data Catalog*, 217, 175
 Buckley, D. A. H., Haberl, F., Motch, C., et al. 1997, *MNRAS*, 287, 117
 Buckley, D. A. H., Sekiguchi, K., Motch, C., et al. 1995, *MNRAS*, 275, 1028
 Channugam, G., Frank, J., King, A. R., & Lasota, J.-P. 1990, *ApJ*, 350, L13
 Channugam, G. & Ray, A. 1984, *ApJ*, 285, 252
 Cropper, M. 1986, *MNRAS*, 222, 225
 Cropper, M. 1990, *Space Science Reviews*, 54, 195
 Cumming, A. 2004, in *ASP Conf. Ser. 315: IAU Colloq. 190: Magnetic Cataclysmic Variables*, ed. S. Vrielmann & M. Cropper, 58
 de Jager, O. C., Meintjes, P. J., O’Donoghue, D., & Robinson, E. L. 1994, *MNRAS*, 267, 577
 de Martino, D., Matt, G., Mukai, K., et al. 2008, *A&A*, 481, 149
 Evans, P. A. & Hellier, C. 2007, *ApJ*, 663, 1277
 Gänsicke, B. T., Marsh, T. R., Edge, A., et al. 2005, *MNRAS*, 361, 141
 Jablonski, F. & Steiner, J. E. 1987, *ApJ*, 323, 672
 Kaluzny, J. & Semeniuk, I. 1988, *Informational Bulletin on Variable Stars*, 3145, 1
 Katajainen, S., Butters, O. W., Norton, A. J., Lehto, H. J., & Piirola, V. 2007, *A&A*, 475, 1011
 Katajainen, S., Piirola, V., Ramsay, G., et al. 2003, *MNRAS*, 340, 1
 King, A. R. 1988, *QJRAS*, 29, 1
 Korhonen, T., Piirola, V., & Reiz, A. 1984, *The Messenger*, 38, 20
 Lamb, D. Q. & Masters, A. R. 1979, *ApJ*, 234, L117
 Landolt, A. U. 1992, *AJ*, 104, 340
 Lehto, H. J. 1997, in *Applications of time series analysis in astronomy and meteorology*, ed. T. Subba Rao, M. B. Priestley, & O. Lessi (London Chapman and Hall)
 Motch, C., Haberl, F., Guillout, P., et al. 1996, *A&A*, 307, 459
 Norton, A. J., Butters, O. W., Parker, T. L., & Wynn, G. A. 2008, *ApJ*, 672, 524
 Norton, A. J., Quaintrell, H., Katajainen, S., et al. 2002, *A&A*, 384, 195
 Osborne, J. P., Rosen, R., Mason, K. O., & Beuermann, K. 1985, *SSRv*, 40, 143
 Patterson, J. 1994, *PASP*, 106, 209
 Patterson, J., Kemp, J., Richman, H. R., et al. 1998, *PASP*, 110, 415
 Penning, W. R., Schmidt, G. D., & Liebert, J. 1986, *ApJ*, 301, 881
 Piirola, V. 1973, *A&A*, 27, 383
 Piirola, V. 1988, *Simultaneous five-colour (UBVRI) photopolarimeter in Polarized Radiation of Circumstellar Origin (Vatican Observatory/University of Arizona Press)*, 735–746
 Piirola, V., Coyne, G. V., & Reiz, A. 1987a, *A&A*, 185, 189
 Piirola, V., Coyne, G. V., & Reiz, A. 1987b, *A&A*, 186, 120
 Piirola, V., Hakala, P., & Coyne, G. V. 1993, *ApJ*, 410, L107
 Piirola, V., Vornanen, T., Berdyugin, A., & Coyne, G. V., S. J. 2008, *ApJ*, 684, 558
 Potter, S. B., Cropper, M., Mason, K. O., Hough, J. H., & Bailey, J. A. 1997, *MNRAS*, 285, 82
 Rosen, S. R., Mittaz, J. P. D., & Hakala, P. J. 1993, *MNRAS*, 264, 171
 Schmidt, G. D., Szkody, P., Smith, P. S., et al. 1996, *ApJ*, 473, 483
 Shakhovskoj, N. M. & Kolesnikov, S. V. 1997, *IAUCirc*, 6760, 2
 Stockman, H. S., Schmidt, G. D., Berriman, G., et al. 1992, *ApJ*, 401, 628
 Swedlund, J. B., Kemp, J. C., & Wolstencroft, R. D. 1974, *ApJL*, 193, L11
 Uslenghi, M., Tommasi, L., Treves, A., Piirola, V., & Reig, P. 2001, *A&A*, 372, L1
 Vaeth, H. 1997, *A&A*, 317, 476
 Vaeth, H., Channugam, G., & Frank, J. 1996, *ApJ*, 457, 407
 Warner, B. 1995, *Cataclysmic Variable Stars* (Cambridge University Press)
 Watts, D. J., Giles, A. B., Greenhill, J. G., Hill, K., & Bailey, J. 1985, *MNRAS*, 215, 83
 Welsh, W. F., Horne, K., & Gomer, R. 1993, *ApJ*, 410, L39
 West, S. C. 1989, *ApJ*, 345, 511
 West, S. C., Berriman, G., & Schmidt, G. D. 1987, *ApJ*, 322, L35
 Wickramasinghe, D. T. & Ferrario, L. 2000, *PASP*, 112, 873
 Wickramasinghe, D. T. & Meggitt, S. M. A. 1985, *MNRAS*, 214, 605
 Zhang, E., Robinson, E. L., Stiening, R. F., & Horne, K. 1995, *ApJ*, 454, 447
 Zharikov, S. V., Tovmassian, G. H., & Echevarría, J. 2002, *A&A*, 390, L23

Table 1. Summary of previously measured circular polarization in IPs.

Name	Wavelength range ^a (nm)	Mean (%)	Min (%)	Max (%)	Integration time (s)	Total time	Ref ¹
AE Aqr	350–920	-0.03 ± 0.02			15	140 min	1
	<i>I</i>	-0.06 ± 0.03			15	150 min	1
	350–570	-0.06 ± 0.02			5	390 min	1
	320–860	$+0.01 \pm 0.02$			$8 \times I^c$	$\times 2$	2
	590–860	-0.01 ± 0.01			1^d	34 min	2
	320–860	-0.13 ± 0.03			$8 \times I^c$	$\times 5$	2
	320–860	$+0.01 \pm 0.01$			$8 \times I^c$	$\times 3$	2
	1150–1350	$+0.06 \pm 0.08$				4 min	2
	1450–1650	-0.80 ± 0.60				7 min	2
	500–750	$+0.07 \pm 0.02$			5	255 min	3
AO Psc	(550)	$+0.06 \pm 0.01$			5	323 min	3
	570–920	$+0.03 \pm 0.03$			240	180 min	1
	<i>I</i>				240	180 min	1
	320–860	-0.05 ± 0.06			$8 \times I^c$	$\times 1$	2
	660–860	$+0.00 \pm 0.07$			$8 \times I^c$	$\times 3$	2
BG CMi	320–860	$+0.03 \pm 0.03$			$8 \times I^c$	$\times 2$	2
	640–860	-0.24 ± 0.03			$2 \times \sim 30$		4
	320–860	-0.05 ± 0.05					5
	720–860	-0.25 ± 0.06					5
	1110–1380(1250)	-1.74 ± 0.26					5
DQ Her	1400–1650(1500)	-4.24 ± 1.78					5
	370–580		-0.6^b	$+0.6^b$	14.2	~ 1980 min	6
EX Hya	320–860	$+0.01 \pm 0.01$				250 min	2
	570–920	-0.02 ± 0.04			240	200 min	1
FO Aqr	590–860	$+0.01 \pm 0.02$			2^d	68 min	2
	640–860	$+0.06 \pm 0.02$					4
GK Per	330–920	-0.01 ± 0.02			120	200 min	1
	<i>I</i>	$+0.11 \pm 0.07$			240	200 min	1
	320–860	-0.06 ± 0.04			$8 \times I^c$	$\times 2$	2
	320–860	$+0.01 \pm 0.04$			$8 \times I^c$	$\times 6$	2
	720–860	-0.01 ± 0.17			$8 \times I^c$	$\times 5$	2
	1150–1350	$+0.19 \pm 0.13$				51 min	2
	1150–1350	$+1.09 \pm 0.31$				141 min	2
	Visual	$+0.11 \pm 0.13$			28	270 min	7
	IR	-0.01 ± 0.55	-0.2^b	$+0.3^b$	28	270 min	7
	1150–1350	$+0.03 \pm 0.10$	-1.3^b	$+0.8^b$		270 min	7
PQ Gem	<i>U</i>	$+0.0 \pm 0.6$				45 min	2
	<i>B</i>	$+0.0 \pm 0.6$				80 min	8
	<i>V</i>	$+0.0 \pm 0.9$				80 min	8
	<i>R</i>		-1.1	$+0.6$		80 min	8
	<i>U</i>		-0.4^b	$+0.3^b$	8×5	162 min	9
	<i>B</i>		-0.3^b	$+0.4^b$	8×5	162 min	9
	<i>V</i>		-0.7^b	$+0.7^b$	8×5	162 min	9
	<i>R</i>		-1.5^b	$+0.7^b$	8×5	162 min	9
	<i>I</i>		-2.7	$+1.5$	8×5	162 min	9
	<i>U</i>		-0.5^b	$+0.3^b$		~ 730 min	10
	<i>B</i>		-0.2^b	$+0.3^b$		~ 730 min	10
	<i>V</i>		-0.6^b	$+0.4^b$		~ 730 min	10
	<i>R</i>		-1.0^b	$+0.2^b$		~ 730 min	10
	<i>I</i>		-1.3^b	$+1.3^b$		~ 730 min	10
	<i>J</i>		-1.2^b	$+1.0^b$		~ 270 min	10
	<i>K</i>		-2.0^b	$+1.3^b$		~ 460 min	10
RXJ2133	(360)	$+0.90 \pm 0.06$	-0.2^b	$+1.5$	4×24	229 min	11
	(440)	$+1.12 \pm 0.05$	$+0.2^b$	$+2.5$	4×24	229 min	11
	(530)	$+1.17 \pm 0.09$	-0.3^b	$+3.5$	4×24	229 min	11
	(690)	$+0.85 \pm 0.07$	$+0.2^b$	$+3$	4×24	229 min	11
	(830)	$+0.89 \pm 0.08$	-0.4^b	$+2.5$	4×24	229 min	11

Table 1. continued.

Name	Wavelength range ^a (nm)	Mean (%)	Min (%)	Max (%)	Integration time (s)	Total time	Ref ¹
TV Col	640–860	-0.03 ± 0.04					4
	320–860	-0.13 ± 0.09			$8 \times I^c$	$\times 1$	2
	320–860	-0.07 ± 0.07			$8 \times I^c$	$\times 3$	2
V1223 Sgr	320–860	-0.08 ± 0.10			$8 \times I^c$	$\times 1$	2
	350–920	-0.06 ± 0.03			240	144 min	1
	<i>I</i> + <i>R</i>	-0.04 ± 0.07			240	563 min	1
	<i>V</i>	-0.48 ± 0.62	≥ -2	$\leq +2$	14		12
	<i>R</i>	$+0.03 \pm 0.13$	≥ -0.5	$\leq +0.5$	14		12
	<i>J</i>	-0.36 ± 0.13	≥ -1	$\leq +0.5$	14		12
	<i>K</i>	$+1.14 \pm 1.26$	≥ -8	$\leq +8$	14		12
V2306 Cyg	(360)	$+0.04 \pm 0.06$			8×10 (210)	872 min	13
	(440)	$+0.16 \pm 0.08$			8×10 (210)	872 min	13
	(530)	$+0.18 \pm 0.11$			8×10 (210)	872 min	13
	(690)	-0.55 ± 0.08	-1.3^b	$+1^b$	8×10 (210)	872 min	13
	(830)	-0.91 ± 0.14	-1.7^b	$+0.4^b$	8×10 (210)	872 min	13
	<i>B</i>	$+0.32 \pm 0.10$	-0.3^b	$+0.7^b$	58	52 min	14
	<i>R</i>	-1.99 ± 0.11	-5.2^b	-0.6^b	45	55 min	14
V2400 Oph	WL		-2.9^b	-1.0^b	120 & 180	~900 min	15
	<i>V</i>	$\sim -1.8^b$	-4.8^b	-1.0^b	120	~33 min	15
	<i>R</i>	$\sim -2.3^b$	-5.1^b	-0.5^b	120	~71 min	15
	<i>I</i>	$\sim -3.3^b$	-6.0^b	-1.0^b	120	~32 min	15
	320–700 (470)	-0.90 ± 0.03			50		16
	560–900 (700)	-2.82 ± 0.04			50		16
V405 Aur	500–750	1.8 (Semi-amp)					17
	<i>U</i>		-2	+2	8×12 (96)	1328 min	18
	<i>B</i>		-3	+3	8×12 (96)	1328 min	18
	<i>V</i>		-3	+3	8×12 (96)	1328 min	18
	<i>R</i>		-2	+2	8×12 (96)	1328 min	18
	<i>I</i>		-1	+1	8×12 (96)	1328 min	18
YY Dra	320–860	$+0.09 \pm 0.10$			$8 \times I^c$	$\times 1$	2

^a Numbers in parentheses indicate the effective wavelength of the filter.^b Estimated from plots.^c *I* corresponds to an unspecified time between 0.5–1 mins.^d Constant polarimeter position.

¹ References - (1) Cropper (1986); (2) Stockman et al. (1992); (3) Beskrovnaya et al. (1996); (4) Penning et al. (1986); (5) West et al. (1987); (6) Swedlund et al. (1974); (7) Berriman et al. (1986); (8) Rosen et al. (1993); (9) Piirola et al. (1993); (10) Potter et al. (1997); (11) Katajainen et al. (2007); (12) Watts et al. (1985); (13) Uslenghi et al. (2001); (14) Norton et al. (2002); (15) Buckley et al. (1995); (16) Buckley et al. (1997); (17) Shakhovskoj & Kolesnikov (1997); (18) Piirola et al. (2008).

Online Material

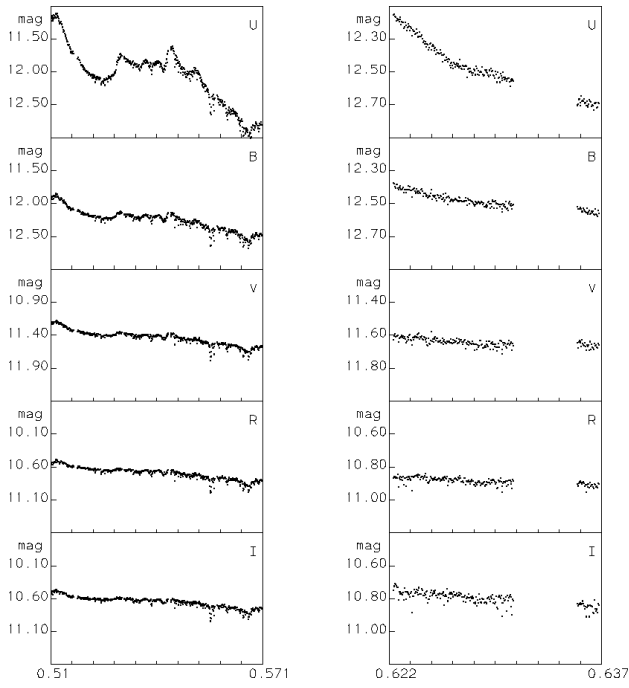


Fig. 1. Raw *UBVR* photometry of AE Aqr taken on the two nights. The abscissa in left plot is $\text{HJD} - 2453949$, in the right plot it is $\text{HJD} - 2453950$.

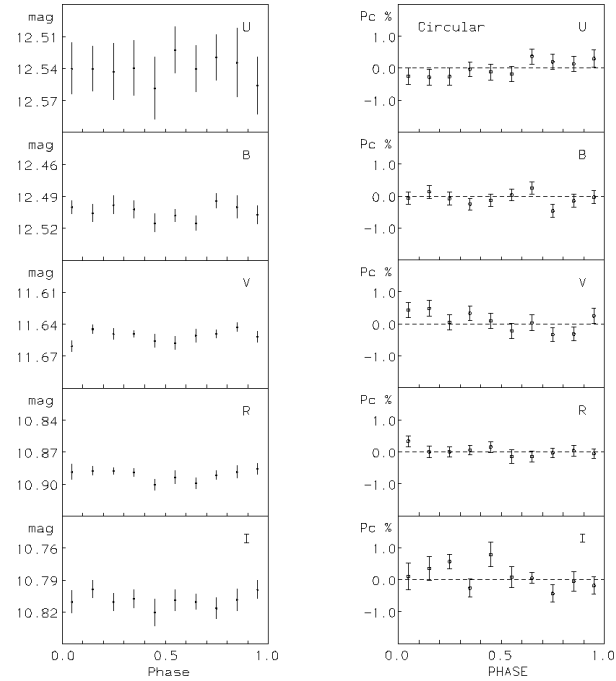


Fig. 3. Spin folded and phase binned simultaneous *UBVR* photometry (left) and circular polarization (right) plots of AE Aqr, taken on the second night ($\text{HJD} 2453950$). Zero phase corresponds to $\text{HJD} 2453949.5$. A spin period of 0.000382833 d was used.

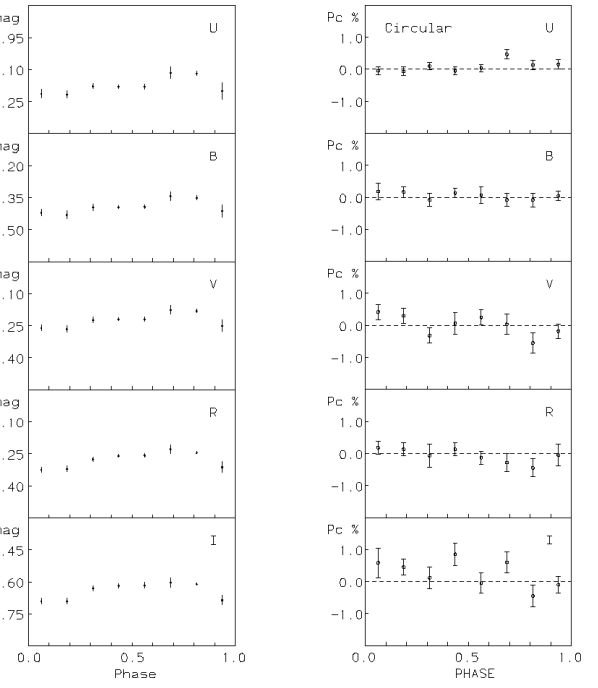


Fig. 4. Spin folded and phase binned simultaneous *UBVR* photometry (left) and circular polarization (right) plots of AO Psc. Circular polarization measurements have an 23 s resolution. Zero phase corresponds to $\text{HJD} 2453949.5$. A spin period of 0.009319484 d was used.

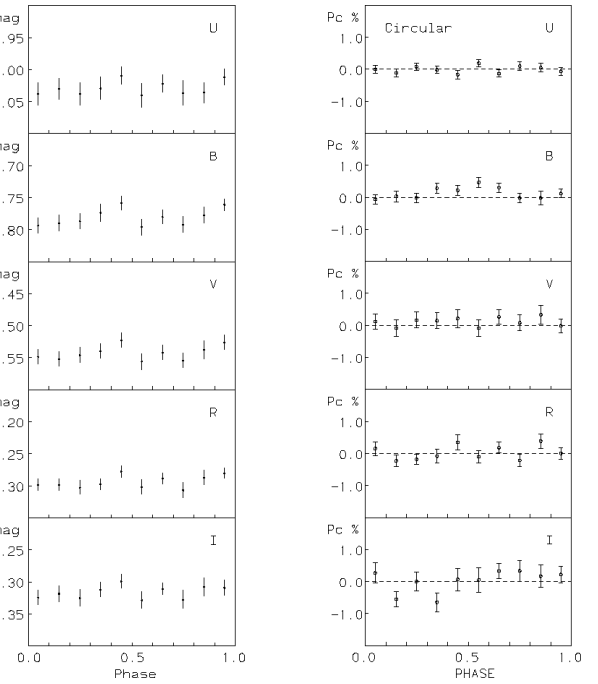


Fig. 5. Spin folded and phase binned simultaneous *UBVR* photometry (left) and circular polarization (right) plots of DQ Her. Zero phase corresponds to $\text{HJD} 2453948.5$. A spin value of 0.00164504 d was used.

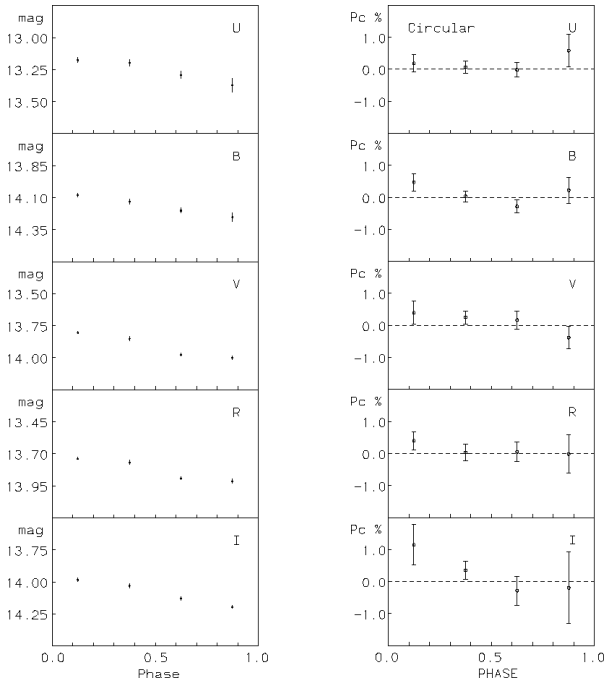


Fig. 6. Spin folded and phase binned simultaneous *UBVR* photometry (left) and circular polarization (right) plots of FO Aqr. Zero phase corresponds to HJD 2453 948.5. A spin period of 0.0014519035 d was used.

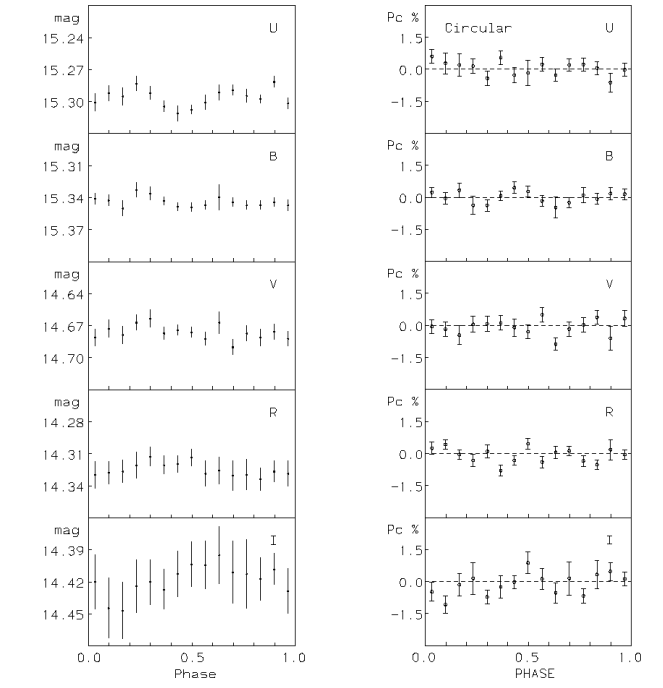


Fig. 10. Spin folded and phase binned simultaneous *UBVR* photometry (left) and circular polarization (right) plots of V2306 Cyg. The spin ephemeris of Norton et al. (2002) was used to phase the spin variations.

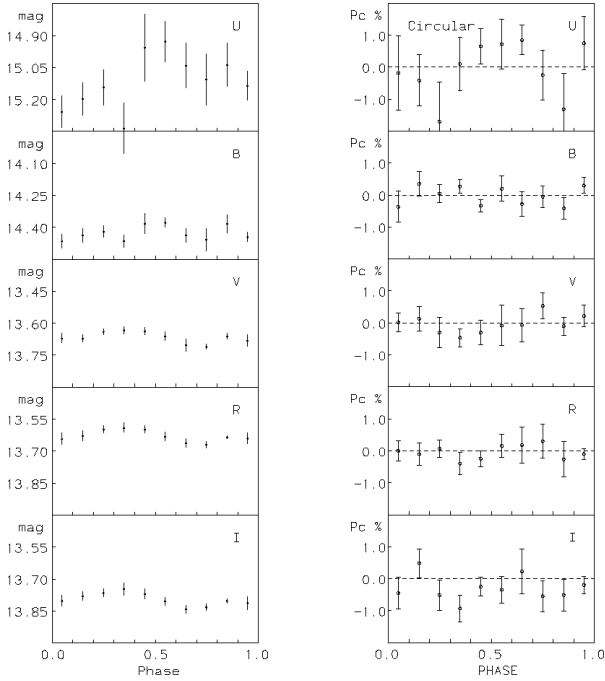


Fig. 9. Spin folded and phase binned simultaneous *UBVR* photometry (left) and circular polarization (right) plots of V1223 Sgr. Zero phase corresponds to HJD 2453 950.5. A spin period of 0.00863 d was used.